High-Performance Nanosensors Based on Plasmonic Fano-like Interference: Probing Refractive Index with Individual Nanorice and Nanobelts

Fernando López-Tejeira,* Ramón Paniagua-Domínguez, and José A. Sánchez-Gil

Instituto de Estructura de la Materia (IEM-CSIC), Consejo Superior de Investigaciones Científicas, Serrano 121, 28006 Madrid, Spain

ABSTRACT

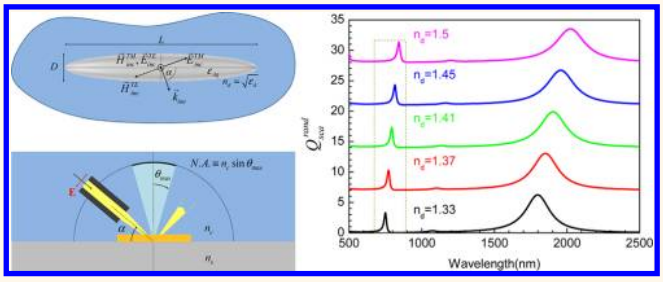

We propose two different configurations for which the Fano-like interference of longitudinal plasmon resonances occurring at individual metallic nanoparticles can be easily employed in refractive index sensing: a colloidal suspension of nanospheroids (nanorice) and a single nanowire with rectangular cross section (nanobelt) on top of a dielectric substrate. We numerically study the performance of the two in terms of their figures of merit, which are calculated under realistic conditions. For the case of nanorice, we explicitly incorporate the effect of size dispersity into the simulations. Our obtained results show that the application of the proposed configurations seems to be not only feasible but also very promising.

KEYWORDS: plasmonics · Fano resonances · individual nanoparticles · nanorice · nanobelts · LSPR sensing

Unlike those propagating at metal/dielectric interfaces,[1−3] localized collective oscillations of charges confined to the surface of metal nanoparticles can be directly excited by external illumination without the need of any additional coupling-in technique, provided that particles are much smaller than the incident wavelength. These oscillations, which can be pictured as a "wave" of electrons moving across the surface of the particle, are referred to as localized surface plasmon resonances (LSPRs), and they are responsible for nanoparticles' bright colors when in colloidal suspension, as a result of their intense absorbing and scattering of light in the visible range.

One of the most appealing properties of LSPRs is that their resonant frequency strongly depends on nanoparticles' size, shape, and composition, as well as on the refractive index of the surrounding medium. Given that present technological advances allow one to control particle geometry down to nanometer scale, spectral shift of LSPRs can then be used to detect extremely small changes of the immediate dielectric environment, for instance, such as those produced by the binding of some biological molecules having a refractive index that is slightly different than that of their solvent.[4−6] Since the pioneering work of Englebienne in 1998,[7] this feature has raised the prospect of LSPR-based sensors to become highly competitive in label-free bioanalytical sensing, as summarized in recent reviews on the subject.[8−10]

When assessing the actual performance of a refractive index sensing scheme based on the spectral shift of a given plasmon resonance, we have to first consider its refractive index sensitivity, which is defined as the linear regression slope within a given range for the position of the resonance (either a peak or a dip) as a function of refractive index. This magnitude is usually expressed in terms of wavelength (S_λ) or energy (S_E) shifts per refractive index unit (RIU), and it provides a preliminary measure of the sensor quality. However, sensitivity alone cannot fully characterize the sensor performance unless ideal conditions are assumed, namely zero system noise and infinitely high spectral resolution. Sherry *et al.*,[11] therefore, proposed the so-called figure of merit (FoM), which is defined as the plasmon resonance sensitivity divided by its "full width at half-maximum" (fwhm), as the most meaningful indicator for evaluating the performance of

* Address correspondence to flt@iem.cfmac.csic.es, flt_jdc@yahoo.es.

Received for review July 9, 2012 and accepted September 6, 2012.

Published online September 06, 2012
10.1021/nn303059s

LSPR-based sensors. Such dimensionless quantity allows one to directly compare the sensing properties of different systems irrespective of their shape, size, and operating wavelength. Hence, it has become a standard benchmark in the field, although alternative figures have also been proposed for fixed-wavelength measurements and thin coating configurations.[12] Although not discussed any further throughout this work, we also have to note that the FoM is inversely proportional to the detection limit of the sensor (that is, the smallest refractive index change that can accurately be measured) assuming the fwhm as a crude approximation of the effective spectral resolution.[13]

According to its very definition, the optimal FoM would then be obtained from those resonances exhibiting both high sensitivity to environment and narrow fwhm, which are precisely the main features of spectral line profiles arising from Fano interference.[14,15] Such an interaction of discrete and continuum-like states (often labeled as "dark" and "bright" modes) has already been employed for refractive index sensing by means of either propagating[16−21] or localized plasmon resonances.[22−28] In this paper, we propose that the Fano-like interference of longitudinal plasmon resonances occurring at individual elongated metallic nanoparticles[29] be employed for refractive index sensing. More precisely, we consider two different single-particle configurations that are easily attainable and, in contrast to some previous proposals,[24,26,28] do not require sophisticated geometrical arrangements at the nanoscale: a colloidal suspension of nanospheroids (nanorice) and a single nanowire with rectangular cross section (nanobelt) on top of a dielectric substrate. We numerically obtain their expected performance in terms of their FoMs, which are calculated under realistic conditions by means of the separation of variables (SVM)[30] and the finite element (FEM)[31] methods (see Methods section for a succinct description of calculation techniques). For the case of colloidal nanorice, we also explicitly incorporate size dispersity into our simulations and discuss its influence on the averaged spectral response.

RESULTS AND DISCUSSION

Colloidal Nanorice. The first configuration we are proposing is based on the sharp peak arising in the scattering spectra of individual Ag nanorice particles (*i.e.*, elongated Ag nanospheroids) as a result of the interference between the fundamental longitudinal LSPR and the next odd-order mode. As discussed in a previous work,[29] such an interaction can be easily understood in terms of a Fano-like interference model where the asymmetry parameter is close to unity, which originates a narrow, asymmetric peak in spectral lines. In order to illustrate this phenomenon, we present in Figure 1a the SVM calculation for the scattering efficiency, Q_{sca}, of a single Ag spheroid with total length L = 345 nm and

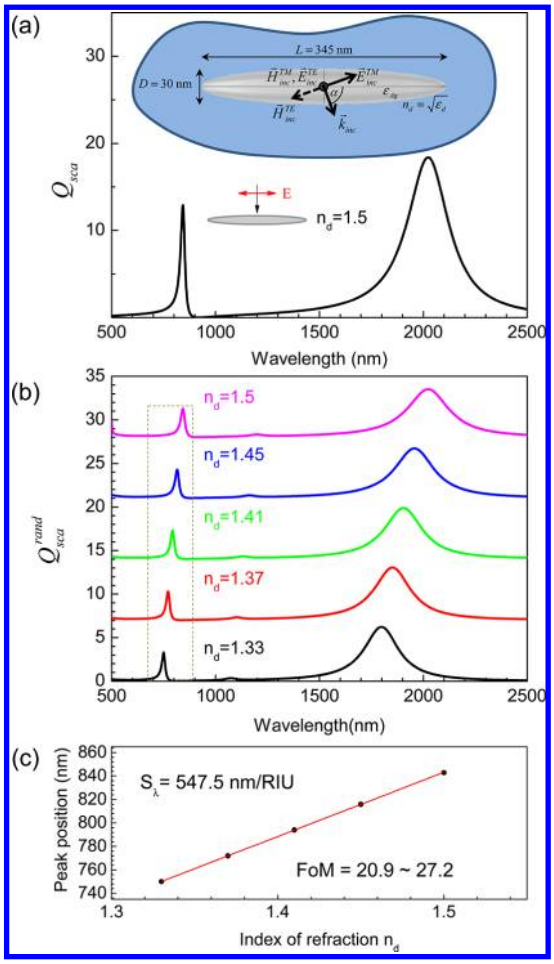

Figure 1. (a) Calculated scattering efficiency of a single Ag spheroid (L = 345 nm; D = 30 nm) surrounded by n_d = 1.5. Incident field is TM-polarized and perpendicular to the rotation axis. (b) Calculated scattering efficiencies for random orientation and different values of n_d. Different curves are artificially shifted for the sake of clarity. (c) Linear scaling of the position of peaks inside the dashed box in panel (a) as a function of n_d. The solid line marks the linear regression curve. Obtained values for S_λ and the range of FoMs are also shown.

maximum diameter D = 30 nm embedded in a dielectric medium with refractive index n_d = 1.5. Light is TM-polarized and impinges perpendicular to the long axis of the spheroid. A broad resonance can be observed in the near-IR at wavelength λ = 2025 nm, whereas an extremely narrow peak appears at λ = 840 nm. This resonance is strongly asymmetric, thus revealing the Fano-like interference involved.

As the position of the longitudinal resonances (being asymmetrical or not) of a metallic nanorod strongly depends on its dielectric environment,[32,33] one can easily envisage a situation where a colloidal suspension of chemically synthesized nanorice[34] can be employed for refractometric sensing.[33,35] However, a proper discussion of such a scenario requires taking into account the possible interparticle coupling, as well as both orientation and polarization issues. With respect to the former, previous works[36−38] have shown

that the most intense interaction between a pair of metallic nanorods arises for their end-to-end aligning along their long axis under TM-polarized light. In such a scenario, the occurrence of interparticle plasmon coupling can be easily monitored by means of the spectral red shift of the dipole-like resonance $\Delta\lambda/\lambda_0$. As we do not have knowledge of any experimental report on plasmon coupling between elongated silver nanoparticles in the near-infrared (NIR) range, let us assume that $\Delta\lambda/\lambda_0$ follows the so-called "plasmon ruler equation" proposed by Jain *et al.*,[38] which has been found to be in good agreement with experimental measurements of silver nanosphere pairs in the same frequency range.[39] Hence, we expect plasmon coupling (and therefore multiple scattering effects) to be negligible for $d/L \gtrsim 0.23$, where d is the interparticle end-to-end separation. Being even more cautious, let us consider $d = 100$ nm to be the minimum acceptable distance for nanorice with $L = 345$ nm. For a cubic cell of size $d + L$, this results in a maximum concentration of $\sim 10^{13}$ particles per milliliter to ensure a dilute regime.

For so well-dispersed nanoparticles, we can assume that their relative spatial and polarization orientations with respect to the incident light are randomly distributed, so that their global response is averaged over all possible TM and TE configurations (see schematic picture in Figure 1a). Therefore, the scattering efficiency for random orientation is given by[32,40,41]

$$Q_{sca}^{rand} \equiv \left\langle \frac{1}{2}\left[Q_{sca}^{TM}(\alpha) + Q_{sca}^{TE}(\alpha)\right]\right\rangle_{\alpha} \quad (1)$$

where the angular brackets $\langle ...\rangle_{\alpha}$ denote averaging over all possible orientation angles α.

In Figure 1b, we explore the evolution of spectral features in Q_{sca}^{rand} as a function of the external refractive index n_d for the same L and D as in panel a. Please notice that different curves are artificially shifted for the sake of clarity. As can be seen for $n_d = 1.5$, probing over oblique incidences produces a global quenching of peaks' intensities, in addition to the emergence of a small signature of the even-order mode between the two. With respect to refractometric sensitivity, it is apparent that the peak located at $\lambda = 840$ nm strongly blue shifts as the refractive index decreases. Nevertheless, its narrow width is preserved for the choice of $\{n_d\}$ values, which are uniformly distributed between those corresponding to water ($n_d = 1.33$) and usual index matching oil ($n_d = 1.5$). For a numerical evaluation of their FoMs, the position of the peaks inside the dashed box is plotted against refractive index in Figure 1c. The resonant wavelength shows a clearly linear dependence on n_d, exhibiting a ± 93 nm shift between the most distant values. The obtained refractive index sensitivity $S_\lambda = 547.5$ nm/RIU results in remarkably high FoMs ranging from 20.9 for $n_d = 1.5$ to 27.2 for $n_d = 1.33$. Hence, the application of the proposed configuration seems to be not only feasible but also very promising.

To end our discussion on the attainability of refractive index sensing by means of colloidal nanorice, let us now focus on the effect of size dispersity in the spectral response of a collection of nanospheroids. As a first approximation, we could consider that the distributions of total length and maximum diameter are statistically independent from each other when their deviations from the mean values $L \equiv 2a_0$;$D \equiv 2b_0$ are small enough.[42] Assuming that the major and minor semiaxes a,b are distributed within the intervals $[a_0 - \Delta a_0, a_0 + \Delta a_0]$ and $[b_0 - \Delta b_0, b_0 + \Delta b_0]$ according to a random process with probability density functions $p(a)$,$q(b)$, respectively, the size-averaged scattering efficiency is given by

$$\tilde{Q}_{sca}^{pol} \equiv \int_{a_0 - \Delta a_0}^{a_0 + \Delta a_0} da p(a) \int_{b_0 - \Delta b_0}^{b_0 + \Delta b_0} db q(b) Q_{sca}^{pol}(a, b) \quad (2)$$

where "pol" denotes either TM or TE polarization. For the sake of simplicity, we impose $p(a)$,$q(b)$ to be Gaussian distributions with means a_0,b_0 and standard deviations σ_a,σ_b defined as

$$\sigma_{a,b} \equiv \frac{\Delta a_0, b_0}{n_{a,b}} \quad (3)$$

with $n_{a,b}$ being integer numbers. Substituting for $\tilde{Q}_{sca}^{pol}$ from eq 2 into eq 1 gives the now size-averaged scattering efficiency for random orientation

$$\tilde{Q}_{sca}^{rand} \equiv \left\langle \frac{1}{2}\left[\tilde{Q}_{sca}^{TM}(\alpha) + \tilde{Q}_{sca}^{TE}(\alpha)\right]\right\rangle_{\alpha} \quad (4)$$

In order to determine the eventual effects of size dispersity in the above-obtained FoMs, we have performed extensive simulations for different values of Δa_0,b_0 and $\sigma_{a,b}$ (see Supporting Information for details). Summing it up, we have concluded that (i) the effect of size dispersion in b is negligible with respect to that of a for the same ratio of mean to standard deviation, as expected from the spectrum's being governed by longitudinal modes, and (ii) that the intensity of the resonance in the most favorable configuration (*i.e.*, TM polarization and normal incidence) decreases down to 50% for $\Delta a_0/a_0 > 0.05$. Given that random orientation additionally quenches the spectra, we have assumed 5% as our operating size dispersion value. Although presently existing samples of silver nanorice are still more disperse (Liang *et al.*[35] report $\Delta a_0/a_0 \sim 0.15$ for $L \sim 300$ nm), we find that such a value falls within the commonly accepted standards of nanoparticle synthesis and could be reasonably attained in the near future.

In Figure 2, we present the calculated $\tilde{Q}_{sca}^{rand}$ in the vicinity of the Fano peak for a single Ag spheroid ($L = 2a_0 = 345$ nm; $D = 2b_0 = 30$ nm) surrounded by $n_d = 1.41$, assuming $\Delta a_0/a_0 = 0.05$;$\Delta b_0 = 0$ and increasing

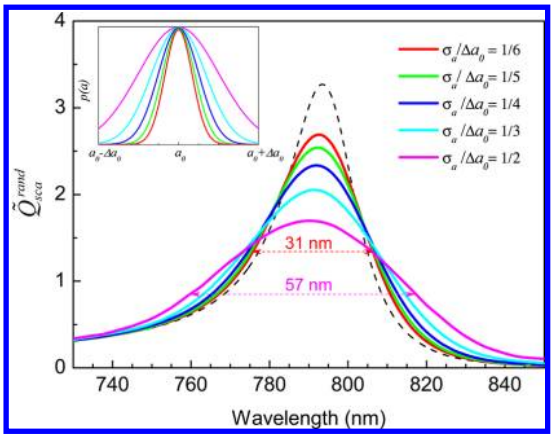

Figure 2. Calculated size-averaged scattering efficiency of a single Ag spheroid ($L = 2a_0 = 345$ nm; $D = 2b_0 = 30$ nm) surrounded by $n_d = 1.41$, assuming random orientation, $\Delta a_0/a_0 = 0.05$ and $\Delta b_0 = 0$. Different solid curves correspond to increasing finite values of standard deviation σ_a. Dashed curve represents the response for a monodisperse distribution. The upper left inset depicts the profiles of probability density function $p(a)$. Maximal and minimal fwhm values are also shown.

values of σ_a (see the upper left inset for $p(a)$ profiles). For the sake of comparison, the calculation for monodisperse spheroids is also shown (dashed curve). We have chosen this precise refractive index as a representative sample of our systematic study on the influence of size dispersity in the figures of merit for the set of values consisting of $\{n_d\} = \{1.33,1.37,1.41,1.45,1.5\}$. As can be seen, increasing standard deviation results in both the flattening and the broadening of the resonance. Hence, the fwhm almost duplicates from $\sigma_a/\Delta a_0 = 0.1666$ to $\sigma_a/\Delta a_0 = 0.5$), although the central wavelength remains nearly unchanged.

Consequently, the effect of size dispersity on the global response over $\{n_d\}$, which is summarized in Table 1, can be considered as neutral form the point of view of refractive index sensitivity. On the other hand, minimal and maximal FoMs (*i.e.*, those corresponding to $n_d = 1.5$ and 1.33, respectively) reduce by half (16.6,18.9 *vs* 8.6,10.2) as $\sigma_a/\Delta a_0$ goes from 0.1666 to 0.5. Remarkably, the obtained values for this latter case are about three times smaller than those of the ideal monodisperse distribution in Figure 1c. However, even for such a worst-case scenario, a FoM ≈ 10 seems to be attainable. This confirms the potential interest of our proposal, especially when comparing this value with those ranging between 2 and 25 that have been recently measured for different realizations of LSPR-based sensors in the NIR range.[22,27,43,44] We note in passing that none of these works discuss the possible effect of size dispersity on the attained figures of merit, which we assume to be a consequence of their use of lithographic (*i.e.*, almost monodisperse) samples. On the other hand, the above-mentioned paper of Liang *et al.*[35] does not report on FoM but on S_λ. Nevertheless, we presume the corresponding figures of merit to be

TABLE 1. Obtained Values of S_λ, Min FoM, and Max FoM for Finite $\sigma_a/\Delta a_0$[a]

$\sigma_a/\Delta a_0$	S_λ (nm/RIU)	min FoM ($n_d = 1.5$)	max FoM ($n_d = 1.33$)
1/6	547.0	16.6	18.9
1/5	541.2	14.6	17.4
1/4	541.2	13.5	15.5
1/3	541.1	11.3	12.9
1/2	541.0	8.7	10.2

[a] $a_0 = 172.5$ nm; $b_0 = 15$ nm; $\Delta a_0/a_0 = 0.05$; $\Delta b_0 = 0.0$; $\{n_d\} = \{1.33,1.37,1.41,1.45,1.5\}$.

smaller than those obtained by us, as far as they are associated with the lowest, dipole-like resonance, which lacks the narrow, asymmetrical line shape originated by Fano-like interference.

Individual Nanobelt on Top of a Dielectric Substrate. Next, we consider the case where an individual metallic nanobelt (that is, a nanowire with rectangular cross section $W \times H$, also referred to as a "nanostripe") is deposited onto a dielectric substrate. In our previous paper,[29] we showed that the scattering spectrum at normal incidence of a metallic nanowire embedded in a dielectric medium is also governed by the Fano-like interference of longitudinal modes, provided that its cross-sectional aspect ratio (cAR $\equiv W/H$) is high enough. However, the assumption of particles being well-dispersed (*i.e.*, non-interacting) in eq 1 seems to be less realistic for actually synthesized gold nanobelts,[45,46] given that they can be described as infinitely long for all practical purposes. Consequently, we will focus our attention on the nanobelt-on-substrate geometry as a simplified version of the nanorod-on-substrate sensing arrangements that have already been experimentally implemented.[47−49]

According to recent reports, gold nanobelts/nanostripes of several tens of nanometers in their cross-sectional height H can be efficiently fabricated by means of either chemical[45,46] or lithographic techniques.[50−53] Assuming $H = 20$ nm to be the operating value, we present in Figure 3a the scattering efficiency calculated by means of FEM for an infinitely long gold rectangular nanowire with $W = 400$ nm that is located on top of a dielectric substrate with refractive index $n_s = 1.5$ and surrounded by a cover medium with $n_c \leq n_s$. Light is TM-polarized and impinges at normal incidence. As previously described by other authors,[22,23] we have defined the excitation by means of the Fresnel coefficients at the interface between cover and substrate semispaces. The scattering efficiencies for $n_c = 1.33$ and 1.5 are then computed by integrating the scattered power over a circumference enclosing the nanobelt.

As can bee seen, the Fano-like interaction between the fundamental resonance and the next odd-order mode does not completely cancel the scattering intensity, unlike that for nanospheroids in Figure 1. Rather, the minimal values are about 40% of those of

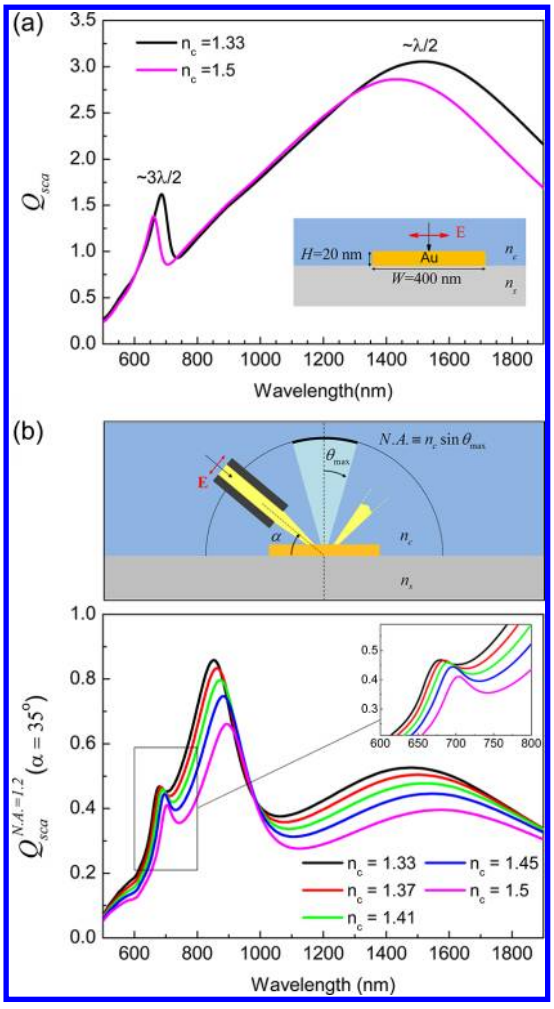

Figure 3. Calculated scattering efficiency of a single Au nanobelt (W = 400 nm; H = 20 nm) located on top of a dielectric substrate with n_s = 1.5 and surrounded by a cover medium with $n_c \leq n_s$. (a) Normal incidence and (b) oblique incidence ($\alpha = 35°$) assuming NA = 1.2. The upper right inset depicts the line profiles at the vicinity of the Fano peak.

the maxima for the broad, dipole-like peaks. Anyway, the position of the resonance red shifts by 25 nm as n_c increases from 1.33 to 1.5, which permits a direct monitoring of the nanobelt's top dielectric environment by means of its scattering spectrum. Given that, at least for lithographic samples, our previous considerations on random orientation and size dispersity can, in principle, be avoided, the nanobelt-on-substrate sensing arrangement seems to be rather attractive, as subsequent odd-order modes (*e.g.*, $\sim 5\lambda/2$) may also be excited. However, although physically sound, the combination of excitation at normal incidence and collection over all angles becomes obviously impractical from the experimental point of view.

In order to obtain realistic estimates, we have then adopted a dark-field-like configuration where the incident light impinges obliquely over the nanobelt and the scattered efficiency is only computed over the arc defined by a given numerical aperture (NA) with respect to the surface normal (see scheme on top of Figure 3b). Assuming NA $\equiv n_c \sin \theta_{max}$ = 1.2, which is typical of water immersion objectives, we present in Figure 3b the corresponding scattering efficiencies calculated at oblique incidence ($\alpha = 35°$) for the same nanobelt and substrate as in panel a and different values of n_c. In contrast to the case of normal incidence and full collection, the lowest even-order resonance is clearly apparent, whereas the dipole-like one is partially suppressed due to the importance of contributions with $\theta > \theta_{max}$. On the other hand, the $3\lambda/2$-like resonance still remains in sight due to its much more anisotropic radiation pattern. Hence, it can be useful for our purposes. The obtained refractive index sensitivity for such configuration within the range [1.33,1.5] is S_λ = 145.7 nm/RIU, which remarkably results in its FoMs ranging from 5.8 for n_c = 1.5 to 9.1 for n_c = 1.33.

Going beyond the proof of principle raises the question of whether there is an optimal configuration that maximizes the figure of merit within a given refractive index range. First of all, the combination of such values with a particular experimental setup will determine the attainable collection and incidence angles. Next, we have to decide the cross-sectional height H (that is the film thickness, lithographically speaking): provided that the nanobelt is wide enough to sustain a $3\lambda/2$-like resonance, its wavelength will scale inversely with H, but no transversal features become apparent in the scattering spectrum for systems with $H \ll W$. Consequently, we can take it just as a fabrication constraint. For a given H, we then have to determine the corresponding minimal cross-sectional width that allows one to reasonably resolve the $3\lambda/2$-like resonance. This requires that the leading contribution to scattering be sufficiently detected by our optical setup. In addition, the operational wavelength range defined by $[\lambda_{res}^{(3)}(n_c = 1.33), \lambda_{res}^{(3)}(n_c = 1.5)]$ both red shifts and widens as cAR increases, given that the position of longitudinal resonances is proportional to W and the refractive index sensitivity S_λ linearly scales as a function of aspect ratio, as one can understand from simple quasi-static considerations.[54] Besides, we have to take into account the evolution of the fwhm values, which may also make S_λ and FoM have an opposite dependence on cAR, as it has already been reported by Becker *et al.*[12]

An illustrative example of this multivariate scenario is presented in Figure 4 for a gold nanobelt with H = 20 nm on top of a dielectric substrate with n_s = 1.5. Open symbols mark the positions of $3\lambda/2$-like resonances in $Q_{sca}^{NA=1.2}(\alpha = 35°)$ for n_c = 1.33 (circles) and n_c = 1.5 (squares) assuming different values of W. As expected, the resulting operational wavelength range both red shifts and widens as cAR increases. With regard to this, we might note in passing that the position of resonances can be fairly well approximated (dashed lines) by a semianalytical effective wavelength model (see Methods section), which has allowed us to optimize our numerical efforts. We have decided W = 400 nm (dotted line) to be the minimal value that

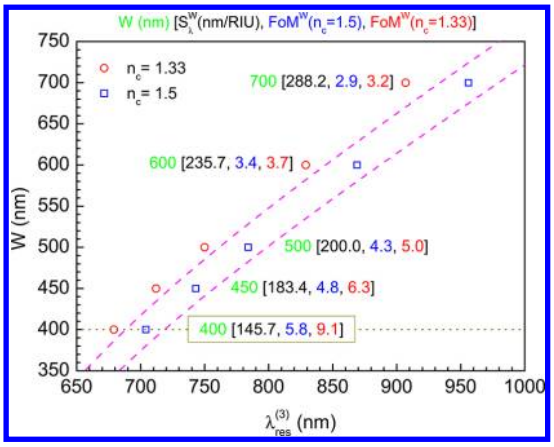

Figure 4. Position of 3λ/2-like resonances in $Q_{sca}^{NA=1.2}(\alpha = 35°)$ as a function of cross-sectional width *W* for a 20 nm high gold nanobelt on top of a dielectric substrate with $n_s = 1.5$ that is covered by a medium with either $n_c = 1.33$ or $n_c = 1.5$. Open symbols render the results of FEM, whereas dashed lines indicate the prediction of a semianalytical effective wavelength model. Dotted line marks the minimal *W* which permits the proper resolution of the peak for $n_c = 1.33$. Obtained values for refractive index sensitivity and minimal and maximal FoMs are also shown.

permits the proper resolution of the peak for $n_c = 1.33$, thus determining the minimal cross-sectional aspect ratio as cAR = 20. For this value, the resonances are all located within the visible range, and they provide both the minimal S_λ and the maximal FoM. For higher cARs, the resonances widen more rapidly than sensitivity rises, so that for $W = 700$ nm, S_λ is almost duplicated with respect to $W = 400$ nm, whereas the values of FoM reduce to less than one-half of the maximal ones (*cf.* square box). Despite such a reduction, we find that $\langle \mathrm{FoM}^{700} \rangle \equiv 1/2(\min \mathrm{FoM}^{700} + \max \mathrm{FoM}^{700}) = 3.0$ is still notable for a single-particle configuration. Summing it up, the designing of a refractive index sensing device based on a nanobelt-on-substrate geometry requires a careful balance between sensitivity, figure of merit, attainable resolution, and operating range. On the other hand, it opens the possibility of the sensor's tailoring to our best convenience.

CONCLUSIONS

We have demonstrated that Fano-like interference of longitudinal plasmon resonances at individual metallic nanoparticles can be employed for refractive index sensing in at least two different configurations. For the first of them (a colloidal suspension of randomly oriented Ag nanorice), we find that a FoM ~ 25 seems to be attainable within the 1.33−1.5 refractive index range. These values are clearly reduced when size dispersity is explicitly taken into account, but we still obtain FoM $\gtrsim 10$ within a 5% size uncertainty. Although such an upper bound for size dispersity is still smaller than that experimentally measured, we expect it to be reasonably feasible with further refinements of nanorice synthesis. As attained, the expected FoMs are fairly as good as (or even better than) those measured for different lithographic realizations of LSPR-based sensors in the NIR range.

In our second proposal (that is, a single Au nanobelt on top of a dielectric substrate), we could, in principle, disregard size dispersity, provided that the sample is obtained by lithographic techniques. On the other hand, the actual implementation of this approach requires the collection of scattered intensity within a finite numerical aperture, which determines the minimal incidence angle for excitation and imposes the minimal cross-sectional width that guarantees a sufficient signal collection for a given metal thickness. Our study for $H = 20$ nm; $W = 400-700$ nm shows that obtained values for the figure of merit and refractive index sensitivity are governed by the nanobelt's geometry, on which they depend oppositely ranging from $S_\lambda^W = 145.7$ nm/RIU, $\langle \mathrm{FoM}^W \rangle = 7.4$ for $W = 400$ nm to $S_\lambda^W = 288.2$ nm/RIU, $\langle \mathrm{FoM}^W \rangle = 3.0$ for $W = 700$ nm. This opens the possibility of their tailoring to one's best convenience.

Finally, we want to remark that we expect our two proposed configurations to be experimentally tested in the near future, as they do not require other nanoscale arrangement than the actual supply of suitable elongated nanoparticles with controlled size dispersity.

METHODS

Calculation Techniques. Calculations for spheroids are performed by means of a modified version of the F77-code made publicly available at the Web site of the Jena-St.Petersburg Database of Optical Constants (JPDOC)[55] in which both eq 1 and eq 4 have been incorporated. A detailed description of SVM formalism can be found in ref 30.

Gaussian probability distribution function for major semiaxis around a_0 is defined as

$$p(a) = Ae^{-(a-a_0)^2/2\sigma_a^2} \quad (5)$$

where $A^{-1} \equiv \sigma_a(2\pi)^{1/2}\mathrm{Erf}[n_a/\sqrt{2}]$ so that

$$\int_{a_0-\Delta a_0}^{a_0+\Delta a_0} da p(a) = 1 \quad (6)$$

For the evaluation of $\tilde{Q}_{sca}^{pol}$ in eq 4, we have used a combination of Romberg's and Gauss-Hermite's numerical quadratures.[56]

Results in Figures 3 and 4 are obtained by using the electromagnetic waves part of the radio frequency module of the finite-element method based COMSOL v4.2 commercial software. The simulation space consisted on a rectangle of width *W* and height *H*, representing the nanobelt section and two concentric circles of radii $R_{in} = 1$ μm and $R_{out} = 1.5$ μm, which generate two subdomains, a circle and an annulus. Those subdomains were further split into two equal parts by a line to represent the glass substrate and the cover medium. The rectangle is located on top of that line and inside the cover medium domain. The two half annulus were set to be cylindrical perfectly matched layers (PML) to absorb all outgoing radiation, each with material properties equal to the adjacent circular subdomain. We have used the scattered field formulation to explicitly write the incident field above the substrate as a sum of

an incident plane wave plus the correspondent component reflected by the interface, whereas only the transmitted component is considered below the substrate. The scattering cross efficiency was computed by integrating the outgoing time-averaged pointing vector of the scattered fields over an auxiliary circumference of radius $R_{aux} = 0.8\ \mu$m and normalizing it by the incident radiation power and the projected cross-sectional width. The presence of an optical instrument aimed to collect the light with a given numerical aperture was simulated by integrating only over the arc length subtended by the maximum angle allowed by that NA in the cover medium.

The meshing process was done with the built-in algorithm of COMSOL. We restricted the mesh to have a maximum element size (MES) of 1 nm for elements along the line representing the interface. The MES represents the maximum size allowed for the edges of the triangles under this restriction. The same MES of 1 nm was imposed for the mesh of the whole nanobelt. In both cases, we imposed a maximum element growth rate (MEGR) of 1.1, meaning that adjacent elements to a given one should not be bigger than 1.1 times the size of it. For all the other domains, a MES of 25 nm was imposed, while keeping the MEGR to 1.1. Multifrontal massively parallel sparse direct solver (MUMPS) was used to solve the resulting linear system, requiring about 6 GB of memory.

The estimates for *W versus* $\lambda_{res}^{(3)}$ in Figure 4 are calculated by means of the resonance condition of a half-wave antenna, assuming the effective wavelength λ_{eff} to be that of the symmetric confined mode propagating across a thin metal film surrounded by two different dielectric media.[57] In addition, the values of *W* have been then corrected in order to take into account the reactance of nanowire ends.[58]

The analytical forms for the dielectric functions of Ag and Au have been obtained by fitting the measured optical data[59] with a sum of Lorentzian terms.

Conflict of Interest: The authors declare no competing financial interest.

Acknowledgment. The research presented in this paper is supported by the Spanish Government (projects Consolider-Ingenio EMET CSD2008-00066 and NANOPLAS FIS2009-11264) and the "Comunidad de Madrid" (MICROSERES network S2009/TIC-1476). R.P.-D. acknowledges support from CSIC through a JAE-Pre grant.

Supporting Information Available: Details on the influence of $\Delta a_0, \Delta b_0$ and $\sigma_{a,b}$ on the size-averaged scattering efficiency of Ag nanospheroids. This material is available free of charge *via* the Internet at http://pubs.acs.org.

REFERENCES AND NOTES

1. Raether, H. *Surface Plasmons on Smooth and Rough Surfaces and on Gratings*; Springer Tracts in Modern Physics; Springer Verlag: Berlin, 1988.
2. Novikov, I.; Maradudin, A. A. Channel Polaritons. *Phys. Rev. B* **2002**, *66*, 1–13.
3. Pile, D. F. P.; Ogawa, T.; Gramotnev, D. K.; Okamoto, T.; Haraguchi, M.; Fukui, M.; Matsuo, S. Theoretical and Experimental Investigation of Strongly Localized Plasmons on Triangular Metal Wedges for Subwavelength Waveguiding. *Appl. Phys. Lett.* **2005**, *87*, 061106.
4. Kreuzer, M. P.; Quidant, R.; Badenes, G.; Marco, M.-P. Quantitative Detection of Doping Substances by a Localised Surface Plasmon Sensor. *Biosens. Bioelectron.* **2006**, *21*, 1345–1349.
5. Kreuzer, M. P.; Quidant, R.; Salvador, J.-P.; Marco, M.-P.; Badenes, G. Colloidal-Based Localized Surface Plasmon Resonance (LSPR) Biosensor for the Quantitative Determination of Stanozolol. *Anal. Bioanal. Chem.* **2008**, *391*, 1813–1820.
6. Aćimović, S. S.; Kreuzer, M. P.; González, M. U.; Quidant, R. Plasmon Near-Field Coupling in Metal Dimers as a Step toward Single-Molecule Sensing. *ACS Nano* **2009**, *3*, 1231–1237.
7. Englebienne, P. Use of Colloidal Gold Surface Plasmon Resonance Peak Shift To Infer Affinity Constants from the Interactions between Protein Antigens and Antibodies Specific for Single or Multiple Epitopes. *Analyst* **1998**, *123*, 1599–1603.
8. Anker, J. N.; Hall, W. P.; Nilam, C.; Zhao, J.; Van, P. Biosensing with Plasmonic Nanosensors. *Nat. Mater.* **2008**, *7*, 442–453.
9. Sepúlveda, B.; Angelomé, P. C.; Lechuga, L. M.; Liz-Marzán, L. M. LSPR-Based Nanobiosensors. *Nano Today* **2009**, *4*, 244–251.
10. Sau, T. K.; Rogach, A. L.; Jäckel, F.; Klar, T. A.; Feldmann, J. Properties and Applications of Colloidal Nonspherical Noble Metal Nanoparticles. *Adv. Mater.* **2010**, *22*, 1805–1825.
11. Sherry, L. J.; Chang, S.-H.; Schatz, G. C.; Van Duyne, R. P.; Wiley, B. J.; Xia, Y. Localized Surface Plasmon Resonance Spectroscopy of Single Silver Nanocubes. *Nano Lett.* **2005**, *5*, 2034–2038.
12. Becker, J.; Trügler, A.; Jakab, A.; Hohenester, U.; Sönnichsen, C. The Optimal Aspect Ratio of Gold Nanorods for Plasmonic Bio-sensing. *Plasmonics* **2010**, *5*, 161–167.
13. White, I. M.; Fan, X. On the Performance Quantification of Resonant Refractive Index Sensors. *Opt. Express* **2008**, *16*, 1020–1028.
14. Luk'yanchuk, B.; Zheludev, N. I.; Maier, S. A.; Halas, N. J.; Nordlander, P.; Giessen, H.; Chong, C. T. The Fano Resonance in Plasmonic Nanostructures and Metamaterials. *Nat. Mater.* **2010**, *9*, 707–715.
15. Giannini, V.; Francescato, Y.; Amrania, H.; Phillips, C. C.; Maier, S. A. Fano Resonances in Nanoscale Plasmonic Systems: A Parameter-Free Modeling Approach. *Nano Lett.* **2011**, *11*, 2835–2840.
16. Tetz, K. A.; Pang, L.; Fainman, Y. High-Resolution Surface Plasmon Resonance Sensor Based on Linewidth-Optimized Nanohole Array Transmittance. *Opt. Lett.* **2006**, *31*, 1528–1530.
17. Henzie, J.; Lee, M. H.; Odom, T. W. Multiscale Patterning of Plasmonic Metamaterials. *Nat. Nanotechnol.* **2007**, *2*, 549–554.
18. Yang, J.-C.; Ji, J.; Hogle, J. M.; Larson, D. N. Metallic Nanohole Arrays on Fluoropolymer Substrates as Small Label-Free Real-Time Bioprobes. *Nano Lett.* **2008**, *8*, 2718–2724.
19. Yanik, A. A.; Huang, M.; Kamohara, O.; Artar, A.; Geisbert, T. W.; Connor, J. H.; Altug, H. An Optofluidic Nanoplasmonic Biosensor for Direct Detection of Live Viruses from Biological Media. *Nano Lett.* **2010**, *10*, 4962–4969.
20. Lee, K.-L.; Wu, S.-H.; Lee, C.-W.; Wei, P.-K. Sensitive Biosensors Using Fano Resonance in Single Gold Nanoslit with Periodic Grooves. *Opt. Express* **2011**, *19*, 24530–24539.
21. Yanik, A. A.; Cetin, A. E.; Huang, M.; Artar, A.; Mousavi, S. H.; Khanikaev, A.; Connor, J. H.; Shvets, G.; Altug, H. Seeing Protein Monolayers with Naked Eye through Plasmonic Fano Resonances. *Proc. Natl. Acad. Sci. U.S.A.* **2011**, *108*, 11784–11789.
22. Lassiter, J. B.; Sobhani, H.; Fan, J. A.; Kundu, J.; Capasso, F.; Nordlander, P.; Halas, N. J. Fano Resonances in Plasmonic Nanoclusters: Geometrical and Chemical Tunability. *Nano Lett.* **2010**, *10*, 3184–3189.
23. Zhang, S.; Bao, K.; Halas, N. J.; Xu, H.; Nordlander, P. Substrate-Induced Fano Resonances of a Plasmonic Nanocube: A Route to Increased-Sensitivity Localized Surface Plasmon Resonance Sensors Revealed. *Nano Lett.* **2011**, *11*, 1657–1663.
24. Pryce, I. M.; Kelaita, Y. A.; Aydin, K.; Atwater, H. A. Compliant Metamaterials for Resonantly Enhanced Infrared Absorption Spectroscopy and Refractive Index Sensing. *ACS Nano* **2011**, *5*, 8167–8174.
25. Liu, S.-D.; Yang, Z.; Liu, R.-P.; Li, X.-Y. High Sensitivity Localized Surface Plasmon Resonance Sensing Using a Double Split NanoRing Cavity. *J. Phys. Chem. C* **2011**, *115*, 24469–24477.
26. Wu, C.; Khanikaev, A. B.; Adato, R.; Arju, N.; Yanik, A. A.; Altug, H.; Shvets, G. Fano-Resonant Asymmetric Metamaterials for Ultrasensitive Spectroscopy and Identification of Molecular Monolayers. *Nat. Mater.* **2012**, *11*, 69–75.

27. Lodewijks, K.; Van Roy, W.; Borghs, G.; Lagae, L.; Van Dorpe, P. Boosting the Figure-of-Merit of LSPR-Based Refractive Index Sensing by Phase-Sensitive Measurements. *Nano Lett.* **2012**, *12*, 1655–1659.
28. Fu, Y. H.; Zhang, J. B.; Yu, Y. F.; Luk'yanchuk, B. Generating and Manipulating Higher Order Fano Resonances in Dual-Disk Ring Plasmonic Nanostructures. *ACS Nano* **2012**, *6*, 5130–5137.
29. López-Tejeira, F.; Paniagua-Domínguez, R.; Rodríguez-Oliveros, R.; Sánchez-Gil, J. A. Fano-like Interference of Plasmon Resonances at a Single Rod-Shaped Nanoantenna. *New J. Phys.* **2012**, *14*, 023035.
30. Voshchinnikov, N. V.; Farafonov, V. G. Optical Properties of Spheroidal Particles. *Astrophys. Space Sci.* **1993**, *204*, 19–86.
31. *COMSOL Multiphysics* v 4.2, RF Module; http://www.comsol.com; accessed September 2012.
32. Khlebtsov, B.; Khlebtsov, N. Multipole Plasmons in Metal Nanorods: Scaling Properties and Dependence on Particle Size, Shape, Orientation, and Dielectric Environment. *J. Phys. Chem. C* **2007**, *111*, 11516–11527.
33. Wei, H.; Reyes-Coronado, A.; Nordlander, P.; Aizpurua, J.; Xu, H. Multipolar Plasmon Resonances in Individual Ag Nanorice. *ACS Nano* **2010**, *4*, 2649–2654.
34. Liang, H.; Yang, H.; Wang, W.; Li, J.; Xu, H. High-Yield Uniform Synthesis and Microstructure-Determination of Rice-Shaped Silver Nanocrystals. *J. Am. Chem. Soc.* **2009**, *131*, 6068–6069.
35. Liang, H.; Zhao, H.; Rossouw, D.; Wang, W.; Xu, H.; Botton, G. A.; Ma, D. Silver Nanorice Structures: Oriented Attachment-Dominated Growth, High Environmental Sensitivity, and Real-Space Visualization of Multipolar Resonances. *Chem. Mater.* **2012**, *24*, 2339–2346.
36. Aizpurua, J.; Bryant, G.; Richter, L.; García de Abajo, F.; Kelley, B.; Mallouk, T. Optical Properties of Coupled Metallic Nanorods for Field-Enhanced Spectroscopy. *Phys. Rev. B* **2005**, *71*, 235420.
37. Jain, P. K.; Eustis, S.; El-Sayed, M. A. Plasmon Coupling in Nanorod Assemblies: Optical Absorption, Discrete Dipole Approximation Simulation, and Exciton-Coupling Model. *J. Phys. Chem. B* **2006**, *110*, 18243–18253.
38. Jain, P. K.; Huang, W.; El-Sayed, M. A. On the Universal Scaling Behavior of the Distance Decay of Plasmon Coupling in Metal Nanoparticle Pairs: A Plasmon Ruler Equation. *Nano Lett.* **2007**, *7*, 2080–2088.
39. Gunnarsson, L.; Rindzevicius, T.; Prikulis, J.; Kasemo, B.; Käll, M.; Zou, S.; Schatz, G. C. Confined Plasmons in Nanofabricated Single Silver Particle Pairs: Experimental Observations of Strong Interparticle Interactions. *J. Phys. Chem. B* **2005**, *109*, 1079–1087.
40. Asano, S.; Sato, M. Light Scattering by Randomly Oriented Spheroidal Particles. *Appl. Opt.* **1980**, *19*, 962–974.
41. Khlebtsov, N. G.; Melnikov, A. G.; Bogatyrev, V. A. The Linear Dichroism and Birefringence of Colloidal Dispersions: Approximate and Exact Approaches. *J. Colloid Interface Sci.* **1991**, *146*, 463–478.
42. Mishchenko, M. I.; Travis, L. D.; Lacis, A. A. *Scattering, Absorption and Emission of Light by Small Particles*; Cambridge University Press: Cambridge, U.K., 2002.
43. Svedendahl, M.; Chen, S.; Dmitriev, A.; Käll, M. Refractometric Sensing Using Propagating *versus* Localized Surface Plasmons: A Direct Comparison. *Nano Lett.* **2009**, *9*, 4428–4433.
44. Offermans, P.; Schaafsma, M. C.; Rodriguez, S. R. K.; Zhang, Y.; Crego-Calama, M.; Brongersma, S. H.; Gómez Rivas, J. Universal Scaling of the Figure of Merit of Plasmonic Sensors. *ACS Nano* **2011**, *5*, 5151–5157.
45. Zhao, N.; Wei, Y.; Sun, N.; Chen, Q.; Bai, J.; Zhou, L.; Qin, Y.; Li, M.; Qi, L. Controlled Synthesis of Gold Nanobelts and Nanocombs in Aqueous Mixed Surfactant Solutions. *Langmuir* **2008**, *24*, 991–998.
46. Anderson, L. J. E.; Payne, C. M.; Zhen, Y.-R.; Nordlander, P.; Hafner, J. H. A Tunable Plasmon Resonance in Gold Nanobelts. *Nano Lett.* **2011**, *11*, 5034–5037.
47. Chen, H.; Shao, L.; Ming, T.; Woo, K. C.; Man, Y. C.; Wang, J.; Lin, H.-Q. Observation of the Fano Resonance in Gold Nanorods Supported on High-Dielectric-Constant Substrates. *ACS Nano* **2011**, *5*, 6754–6763.
48. Ament, I.; Prasad, J.; Henkel, A.; Schmachtel, S. Single Unlabeled Protein Detection on Individual Plasmonic Nanoparticles. *Nano Lett.* **2012**, *12*, 1092–1095.
49. Zijlstra, P.; Paulo, P. M. R.; Orrit, M. Optical Detection of Single Non-absorbing Molecules Using the Surface Plasmon Resonance of a Gold Nanorod. *Nat. Nanotechnol.* **2012**, *7*, 379–382.
50. Muskens, O. L.; Giannini, V.; Sanchez-Gil, J. A.; Gómez Rivas, J. Strong Enhancement of the Radiative Decay Rate of Emitters by Single Plasmonic Nanoantennas. *Nano Lett.* **2007**, *7*, 2871–2875.
51. Neubrech, F.; Weber, D.; Lovrincic, R.; Pucci, A.; Lopes, M.; Toury, T.; de La Chapelle, M. L. Resonances of Individual Lithographic Gold Nanowires in the Infrared. *Appl. Phys. Lett.* **2008**, *93*, 163105.
52. Neubrech, F.; Weber, D.; Enders, D.; Nagao, T.; Pucci, A. Antenna Sensing of Surface Phonon Polaritons. *J. Phys. Chem. C* **2010**, *114*, 7299–7301.
53. Cattoni, A.; Ghenuche, P.; Decanini, D.; Chen, J.; Pelouard, J.-l. λ^3/1000 Plasmonic Nanocavities for Biosensing Fabricated by Soft UV Nanoimprint Lithography. *Nano Lett.* **2011**, *11*, 3557–3563.
54. Lee, K.-S.; El-Sayed, M. A. Gold and Silver Nanoparticles in Sensing and Imaging: Sensitivity of Plasmon Response to Size, Shape, and Metal Composition. *J. Phys. Chem. B* **2006**, *110*, 19220–19225.
55. http://www.astro.spbu.ru/JPDOC as of September 6 2012.
56. Press, W. H.; Teukolsky, S. A.; Vetterling, W. T.; Flannery, B. P. *Numerical Recipes in Fortran 77: The Art of Scientific Computing (Vol. 1 of Fortran Numerical Recipes)*, 2nd ed.; Cambridge University Press: Cambridge, U.K., 1997.
57. Burke, J.; Stegeman, G.; Tamir, T. Surface-Polariton-like Waves Guided by Thin, Lossy Metal Films. *Phys. Rev. B* **1986**, *33*, 5186–5201.
58. Schelkunoff, S. A. Theory of Antennas of Arbitrary Size and Shape. *Proc. IRE* **1941**, *29*, 493–521.
59. Johnson, P.; Christy, R. Optical Constants of the Noble Metals. *Phys. Rev. B* **1972**, *6*, 4370.